4H-SiC Surface Modified by a Green Femtosecond Laser at Low Fluence

Yi-Hsien Liu and Chung-Wei Cheng[*]

Department of Mechanical Engineering, National Yang Ming Chiao Tung University, No. 1001, Ta Hsueh Road, Hsinchu 300, Taiwan
[*]Corresponding author's email:weicheng@nycu.edu.tw

This study used a single femtosecond laser pulse with a wavelength of 515 nm to irradiate the 4H-SiC sample surface. The pulse energy was 1740-2110 nJ, and the effective fluence was around 1.27-1.54 J/cm^2. The ablation threshold is 1.26 J/cm^2. The surface morphology and the ablation depth were measured by scanning electron microscopy (SEM) and atomic force microscope (AFM). The ablation depth is around 12 nm. On the other hand, a simplified model with a two-temperature model and dynamic optical model was used to predict the ablation threshold. The simulation result shows that the ablation threshold is around 1.2 J/cm^2, which is matched the experimental results.
Keywords: femtosecond laser; single pulse; low fluence ablation; silicon carbide (SiC)

1. Introduction

Silicon carbide (SiC) has attracted more attention because it has many advantages, such as wide bandgap and high thermal conductivity. It has been gradually used in the electronic industry, such as high-power devices. Femtosecond laser has been widely used in the industry because it has some advantages, such as small heat-affected zone and high peak power intensity. The high peak power intensity can induce non-linear absorption, which is very suitable for processing the wide-bandgap material. Therefore, many studies have investigated the SiC process and application [1-8]. Z. U. Rehman et al. [3] investigated the structural transformation of 6H-SiC after irradiating by different pulse energy. The ablation area was checked by atomic force microscope (AFM), Raman, and transmission electron microscopy (TEM) measurement. They discovered that an amorphous layer forms on the single-crystal silicon carbide with a thickness of approximately 50 nm. H. Shi et al. [4] used a single femtosecond laser pulse with different pulse energy to irradiate SiC. The threshold of melting, structural transformation, and residual stress were investigated. Y.C. Liang et al. [8] generated a low spatial frequency laser-induced periodic surface structures (LIPSS) on the 4H-SiC surface with relatively low power input. The high-quality structures can be obtained after the chemical etching is conducted. In simulations, the two-temperature model (TTM) often integrates with the carrier density model to characterize the interaction between femtosecond lasers and silicon carbide [9,10]. Z. Yan et al. [9] utilized the TTM and the dynamic optical model to predict the period of LIPSS produced by a 1030 nm femtosecond laser. They also suggested that SiC begins to decompose when its surface temperature reaches the melting point. G. Tsibidis et al. [10] discussed the carrier dynamics generated by a femtosecond laser with a 400 nm wavelength at varying laser fluences. They provided insights into the dynamic optical properties and carrier density for different fluences. Additionally, they noted that SiC decomposition occurs when the surface temperature approaches the melting point.

Many studies have investigated the different phenomena that occurred with the different laser power inputs, such as ablation, phase transformation, and LIPSS. However, there is less study focused on using a single pulse femtosecond laser to irradiate the 4H-SiC with the fluence that is close to the ablation threshold. In addition, the ablation profile and ablation depth obtained by a single femtosecond laser are rarely presented.

In this study, a single green femtosecond laser pulse was used to irradiate 4H-SiC. The input laser fluence was controlled near the ablation threshold. The ablation threshold and surface morphology were checked. On the other hand, a simplified model with the TTM and dynamic optical model was used to check the ablation threshold.

2. Experimental setup

An N-type 4H-SiC wafer (Atecom, Inc.) with a thickness of 350 μm was used in this study. The Si-face was irradiated in this study. The femtosecond laser (KASMORO, mRadian Inc.) with a wavelength of 515 nm, a pulse duration of 221 fs, and a repetition rate (f_{rep}) of 100 kHz. The output beam is 2 mm ($1/e^2$), and the maximum power is 1.8 W. The output laser beam is reflected by a series of reflective mirrors and passes through the Galvanometer scanner, and is focused by a telecentric lens (f=67 mm). The schematic diagram of the laser system is shown in Fig. 1(a). In this study, the single pulse irradiation was achieved by the high scanning speed. The five different scanning speeds (1600-2000 mm/s) with the repetition rate of 100 kHz were tested to ensure the single shot can be obtained. And finally, the 2000 mm/s was used in this study. The schematic diagram of the laser process is shown in Fig. 1(b). Fig. 1(c) represents the scanning electron microscope (SEM) images of the scanning process. The result shows that the laser spot can be separated when the scanning speed is 2000 mm/s. A single pulse can be achieved.

In this study, the effective spot size is determined by the D^2 method proposed by [11]. The area we choose to conduct the D^2 method is the ablation area which is in the center of the irradiation area, as shown in the green circle in Fig. 4 (a). The power meter (919P-050-26, Newport) was used to measure the laser average power. The laser power (P) used in this study was around 174-211 mW. The pulse

energy (E_J) can be calculated by $E_J = P/f_{rep}$. The f_{rep} was 100 kHz and the pulse energy and be calculated around 1740-2110 nJ. The effective spot size is around 18.71 μm. The effective fluence can be determined and is around 1.27-1.54 J/cm².

After processing, the sample was cleaned by the ultrasonic beat with alcohol and deionized water for 10 min. Scanning electron microscopy (SEM, Hitichi-8010) was used to check the surface morphology. The atomic force microscope (AFM, Bruker-Edge) and the confocal were used to check the surface profile and measure the ablation depth.
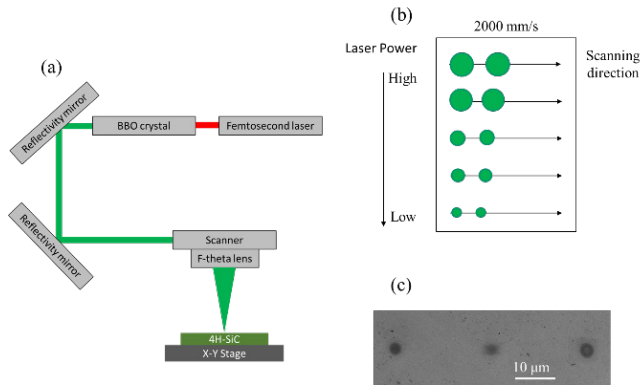
Fig. 1 (a) The schematic diagram of the laser system, (b) the schematic diagram of the scanning process, (c) the SEM image obtained by using laser power is 174 mW and the scanning speed is 2000 mm/s

3. Modeling

During the laser irradiation to SiC, the carrier can be excited and transit from the valence band to the conduction band by non-linear absorption. In this study, due to the wavelength we used was 515 nm, which can induce the two-photon absorption in the process. Thus, we tried to use the Boltzmann-transport equation to describe the dynamic carrier density:

$$\frac{\partial n_e}{\partial t} = \frac{\alpha I(z,t)}{h\omega} + \frac{\beta I(z,t)^2}{2h\omega} - \gamma n_e^3 + \theta n_e \qquad (1)$$

the first and second terms are single and two-photon absorption. The γ and θ are the Auger recombination coefficient and impact ionization coefficient. n_e is carrier density.

During lasing, the optical properties are varied with the n_e. The dynamic optical properties must be considered in the model to enhance the accuracy. The Drude model can be used to calculate the dynamic dielectric constant after obtaining the n_e by Eq. (1). The Drude model is shown below:

$$\varepsilon(n_e) = \varepsilon_{rt} + \frac{-e^2 n_e \tau_D}{\varepsilon_0 m_{opt}^* m_e \omega(i + \omega\tau_D)} \qquad (2)$$

where ε_{rt} is the dielectric constant at room temperature, e is the electron charge, ε_0 is the vacuum permittivity, m_{opt}^* is the effective optical mass, m_e is the electron mass, τ_D is the damping time, and ω is the laser frequency. After the dielectric constant is obtained by Eq. (2), the refractive index, extinction coefficient, reflectivity, and free-carrier

absorption can be obtained. The detailed formula can refer [12].

Assuming that the laser is normal to the sample surface, the surface laser intensity can be described by:

$$I(0,t) = 0.94 \times \frac{[1-R(0,t)] \times F}{t_p} \cdot exp^{-2.77(\frac{t}{t_p})^2} \qquad (3)$$

where the $R(0,t)$ is the surface reflectivity determined by Eq., F is the laser fluence, and t_p is the FWHM pulse duration of Gaussian pulse.

When the laser intensity propagates into the material along with the z-axis, the laser attenuation can be obtained by solving the following ordinary differential equation:

$$\frac{\partial I(z,t)}{\partial z} = -(\alpha_{SPA} + \alpha_{FCA})I - \beta I^2 \qquad (4)$$

where the α_{SPA} is the single-photon absorption coefficient, the α_{FCA} is the free-carrier absorption coefficient, and the β is the two-photon absorption coefficient.

In summary, the total laser heat source term can be expressed as follows:

$$S(z,t) = \alpha_{total}I(z,t) \qquad (5)$$

where the α_{total} is the $\alpha_{SPA} + \alpha_{FCA}$ and the $I(z,t)$ is the intensity along with the z-axis depending on the dynamic optical properties.

After the heat source term is determined by Eq. (5), the two-temperature model can be used to calculate the temporal electron and lattice temperature, which is shown in below:

$$C_e \frac{\partial T_e}{\partial t} = \nabla(K_e \nabla T_e) - G(T_e - T_l) + S \qquad (6)$$

$$C_l \frac{\partial T_l}{\partial t} = \nabla(K_l \nabla T_l) + G(T_e - T_l) \qquad (7)$$

where the C, K, and G are the heat capacity, thermal conductivity, and electron-lattice coupling factor, respectively. The subscripts e and l are represented by electron and lattice, respectively.

In the numerical simulation, the laser pulse duration is set at 221 fs. The laser pulse starts at 0, reaches the maximum at 3 t_p, and ends at 6 t_p. The initial T_e and T_l are set at 300 K. The n_e is set at $10^{12} cm^{-3}$. The ablation criterion was set at the melting temperature [10] (3003 K at 4H-SiC). All the parameters used to calculate the carrier density, dynamic optical, electron, and lattice temperature can be seen in [9,10].

4. Results and discussion

Fig. 2 presents the temporal electron, lattice temperature and carrier density at 1.2 J/cm². As shown in Fig. 2(a), the trend of electron temperature and carrier density are the same. They increased with the laser input and reached the maximum at 0.39 and 0.7 ps and then started to decrease. On the other hand, the lattice temperature starts to increase at 0.3 ps and then exceeds the ablation criterion (melting temperature =3003 K) at 1.54 ps.
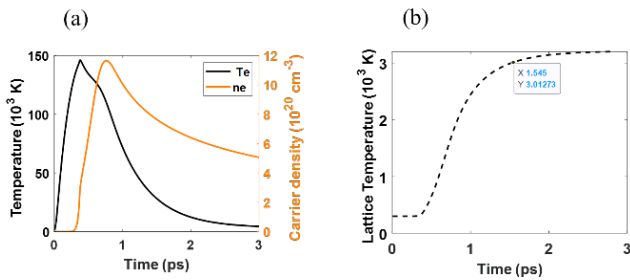
Fig. 2 The temporal electron, lattice temperature, and carrier density obtained by 1.2 J/cm²

Fig. 3 presents the semi-logarithmic plot of the single pulse fluence against the square of ablation width. The straight line was obtained by curve-fitting from experimental data. The ablation threshold is 1.26 J/cm² which is high than the melting threshold (0.31 J/cm²) and lower than the structural transformation threshold (3.44 J/cm²) proposed by [4]. The ablation threshold calculated by experimental results was matched with the simulation results (1.2 J/cm²).
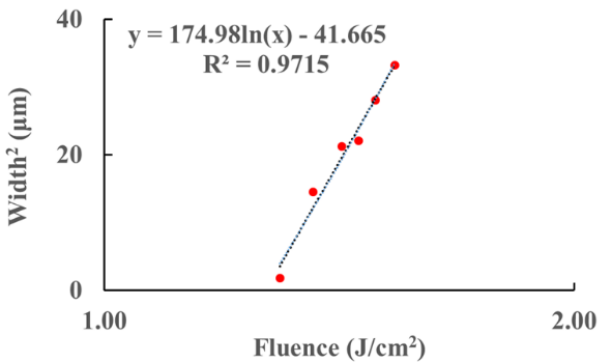

Fig. 3 The laser fluence against ablation width
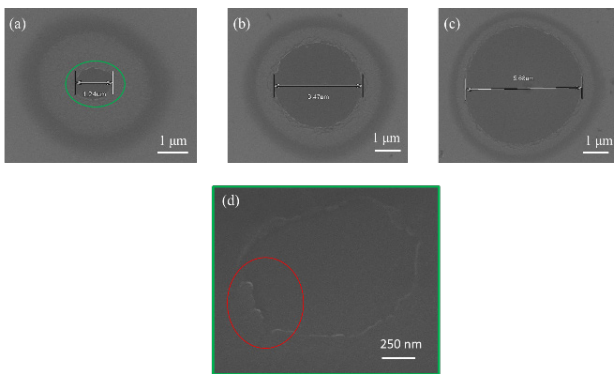
Fig. 4 The SEM images of irradiation area obtained by different laser fluence: (a) 1.3 J/cm², (b) 1.36 J/cm², (c) 1.54 J/cm², and (d) is the magnification of (a)

Fig. 4 presents the surface morphology obtained by different laser fluences (1.3, 1.36, and 1.54 J/cm²). Fig. 4(d) is the magnification area of Fig. 4(a). There are three different areas that can be observed in the irradiation area. The phenomenon is similar to the previous results [4]. The ablation phenomenon can be observed in the center of the irradiation area. The width of the ablation area is increased with the fluence increase. The widths are 1.24, 3.57, and 5.68 µm. As shown in Fig. 4(d), the spallation effect can be observed at the edge of the ablation area (red circle). The

ablation mechanism is similar to the other brittle material, such as silicon [13].

In this study, we tried to find the smallest ablation depth obtained by the lowest fluence input. Therefore, the AFM measurement was used to scan the whole laser irradiation area. Fig. 5 presents the AFM images of the laser irradiation area obtained by 1.3 J/cm². Fig. 5(a) is the AFM scanning area, and Fig. 5(b) is the ablation profile. The results show that the ablation area is very flat, and the ablation depth is around 12 nm. The ablation profile is fascinating because the beam profile used in this study is Gaussian rather than flat-top. The profile is different from the other drilling processes, whether metal [14] or semiconductors [15,16]. However, the ablation profile is really similar to the thin film removed from the substrate. Note that the native-oxide layer on the SiC surface is around 3-10 nm, which is close to the ablation depth we obtained from AFM. However, more measurements must be conducted to determine whether it is the native oxide layer that has been removed or the SiC that has been removed, such as X-ray photoelectron spectroscopy (XPS) or TEM.

According to the results shown in Fig. 5, a small ablation depth can be obtained by controlling the fluence input near the ablation threshold. It can be extended to a large area with selective ablation. An array with a nanometer ablation depth can be obtained.
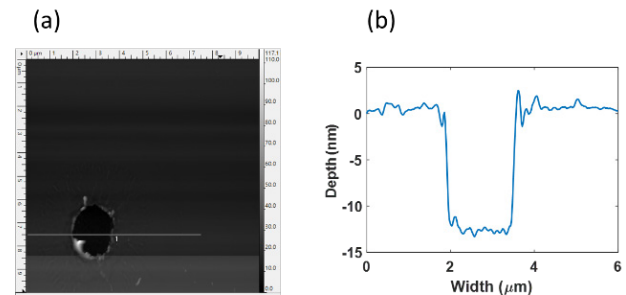
Fig. 5 The AFM images of the irradiation area were obtained by using 1.3 J/cm². (a) the scanning area; (b) the cross-section profile

5. Conclusion

In this study, a single femtosecond laser pulse with a wavelength of 515 nm was used to irradiate 4H-SiC. A model with TTM model, a dynamic optical model was used to check the ablation threshold. The results show that when the input power is 1.2 J/cm², the SiC is ablation. On the other hand, the ablation threshold was 1.26 J/cm². The width of the ablation area is increased with the laser fluence increased. The depth of the ablation area obtained by using 1.3 J/cm² is around 12 nm. Interestingly, the bottom of the ablation area is flat. It can be deduced that the native oxide layer that existed on the sample surface was removed. The simulation results are matched with the experimental results.

References

[1] C. Wang, S. Kurokawa, T. Doi, J. Yuan, Y. Sano, H. Aida, K. Zhang, and Q. Deng: ECS J Solid State Sci Technol, 6, (2017) 105.

[2] E. Kim, Y. Shimotsuma, M. Sakakura, and K. Miura: Opt. Mater. Express, 7, (2017) 2450.

[3] Z. U. Rehman and K. A. Janulewicz: Appl. Surf. Sci., 385, (2016) 1.

[4] H. Shi, Q. Song, Y. Hou, S. Yue, Y. Li, Z. Zhang, M. Li, K. Zhang, and Z. Zhang: Ceram. Int., 48, (2022), 24276.

[5] L. Wang, Y. Zhao, Y. Yang, M. Zhang, and Y. Zhao: Micromachines, 13, (2022) 1291.

[6] K. Vanthanh, Y.C. Ma, J. H. Si, T. Chen, F. Chen, and X. Hou: Chin. Phys. Lett., 31, (2014) 037901.

[7] Y. H. Liu, K. K. Kuo, C. W. Cheng, and A. C. Lee: Opt. Laser Technol., 151, (2022) 108081.

[8] Y.C. Liang, Y.E. Li, Y.H. Liu, J.F. Kuo, C.W. Cheng, and A.C. Lee: Opt. Laser Technol., 163, (2023) 109437.

[9] Z. Yan, G. Li, Y. Zhang, W. Wang, and X. Mei: Appl. Phys. A., 126, (2020) 1.

[10] G. Tsibidis, L. Mouchliadis, M. Pedio, and E. Stratakis: Phys. Rev. B, 101, (2020) 075207.

[11] J. Liu: Opt. Lett., 7, (1982) 196.

[12] Y. H. Liu and C. W. Cheng: J. Manuf. Mater. Process., 7, (2023) 68.

[13] A. Ionin, S. Kudryashov, L. Seleznev, D. Sinitsyn, A. Bunkin, V. Lednev, and S. Pershin: J. Exp. Theor. Phys., 116, (2013) 347.

[14] Y. H. Liu and C. W. Cheng: Opt. Commun., 509, (2021) 127875.

[15] R. Moser, M. Domke, J. Winter, H. P. Huber, and G. Marowsky: Adv. Opt. Technol., 7, (2018) 255.

[16] C. Wang, S. Kurokawa, J. Yuan, L. Fan, H. Lu, Z. Wu, W. Yao, K. Zhang, Y. Zhang, and T. Doi: Int. J. Autom., 12, (2018) 187.